PHYSICAL REVIEW D VOLUME 27, NUMBER 4 15 FEBRUARY 1983

Eighth-order magnetic moment of the electron. I. Second-order vertex containing second-, fourth-, and sixth-order vacuum polarization subdiagrams

T. Kinoshita and W. B. Lindquist*
Newman Laboratory of Nuclear Studies, Cornell University, Ithaca, New York 14853
(Received 25 March 1982)

We have calculated the contribution to the eighth-order anomalous magnetic moment of the electron arising from 25 Feynman diagrams generated by inserting second-, fourth-, and sixth-order vacuum polarization loops in the photon line of the second-order vertex diagram. Our result is $0.0766(6)(\alpha/\pi)^4$. The theoretical error represents the estimated accuracy (90% confidence limit) of the numerical integrations.

I. INTRODUCTION AND SUMMARY

The anomalous magnetic moment of the electron, $a_e=(g_e-2)/2$, has always played a central role in testing the validity of quantum electrodynamics (QED). At present the best published experimental values of the anomalous magnetic moment of the electron and positron are[1,2]

$$a_{e^-}^{\rm exp}=1\,159\,652\,200(40)\times10^{-12}\,,\qquad a_{e^+}^{\rm exp}=1\,159\,652\,222(50)\times10^{-12}\,. \tag{1.1}$$

The agreement between the values in (1.1) affirms the validity of the *TCP* theorem for the electron g factor to the level of 10^{-10}.

The QED prediction for a_e can be written as a power series in α/π,

$$a_e^{\rm QED}=C_1(\alpha/\pi)+C_2(\alpha/\pi)^2+C_3(\alpha/\pi)^3+C_4(\alpha/\pi)^4+\cdots\,. \tag{1.2}$$

The first three coefficients have been calculated,[3,4]

$$C_1=0.5\,,\qquad C_2=-0.328\,478\,445\cdots\,,\qquad C_3=1.176\,5(13)\,. \tag{1.3}$$

If one uses the best current value[5] of the fine-structure constant

$$\alpha^{-1}=137.035\,963(15)\,, \tag{1.4}$$

the QED prediction (1.3), including other known small corrections,[3] leads to

$$a_e^{th}=1\,159\,652\,478(127)(17)(?)\times10^{-12}\,. \tag{1.5}$$

The first error quoted is due to the experimental error in (1.4), the second is due to the purely computational error in C_3, and the third (?) refers to the error of the yet-to-be-calculated eighth-order contribution. If one ignores this last uncertainty, the agreement between (1.5) and (1.1) is at the two-standard-deviations level.

The error in C_3 arises from the 21 integrals (out of 72) which are not yet known analytically. Of these, 16 have been evaluated recently by a combined analytic-numerical technique[4] and contribute negligible error. The error in the remaining five will be reduced soon, either by the analytic-numerical technique,[6] or by pushing the purely numerical integration harder.

In view of the magnitude of $(\alpha/\pi)^4$, which is about 29×10^{-12}, it is obvious that the largest, theoretically accessible error is that of C_4. In 1977, long before some of these results became available, we conducted a feasibility study of the eighth-order calculation and found it to be possible to complete within a reasonable amount of time and effort.[7] Fortified by this result, we launched upon a systematic evaluation of C_4. This is the first of a series of five papers on our calculation.

There are altogether 891 Feynman diagrams contributing to the electron anomaly in the order α^4. These diagrams can be classified into five (gauge-invariant) groups according to the way vacuum polarization subdiagrams appear in them.

Group I: second-order vertex diagram containing vacuum polarization loops of second, fourth, and sixth orders. Twenty-five diagrams belong to this group. Typical diagrams are shown in Fig. 1(a).

Group II: fourth-order vertex diagrams containing vacuum polarization loops of second and fourth orders. This group contains 54 diagrams. Typical diagrams are shown in Fig. 1(b).

Group III: sixth-order vertex diagrams containing a vacuum polarization loop of second order. One

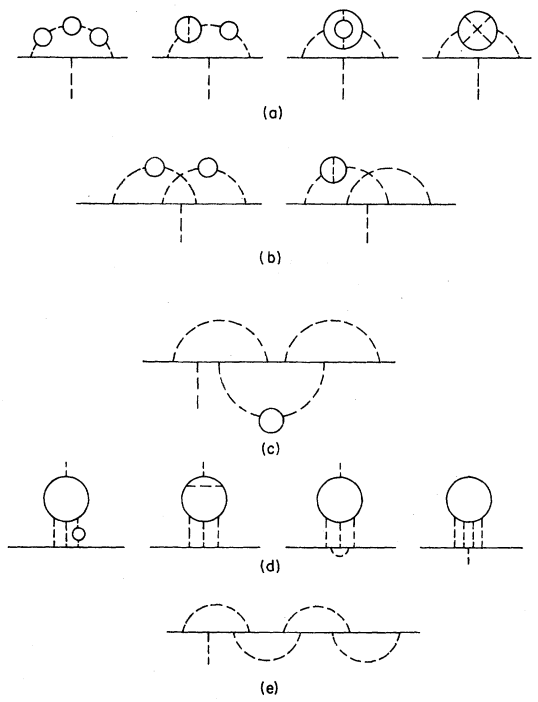

FIG. 1. Typical vertex diagrams of eighth order from the five groups contributing to C_4.

hundred fifty diagrams belong to this group. A typical diagram is shown in Fig. 1(c).

Group IV: vertex diagrams containing a photon-photon scattering subdiagram with further radiative corrections of various kinds. This group consists of 144 diagrams. Typical diagrams are shown in Fig. 1(d).

Group V: diagrams that contain no vacuum polarization loops. This group is comprised of 518 diagrams. A typical diagram is shown in Fig. 1(e).

We report here the contribution to a_e from the 25 diagrams of group I. It is convenient to further classify these diagrams into the following gauge-invariant subgroups.

Subgroup I(a): a single diagram obtained by inserting three second-order vacuum polarization loops in a second-order vertex. This is shown at the left end of Fig. 1(a).

Subgroup I(b): diagrams obtained by insertion of a second- and fourth-order vacuum polarization loop in a second-order vertex. Six diagrams belong to this group. Three are shown in Fig. 2. The other three are obtained from them by time reversal.

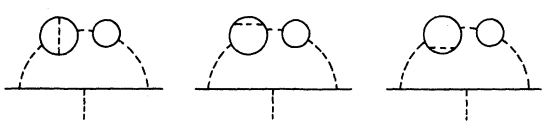

FIG. 2. Three of the diagrams contributing to subgroup I(b). The other three are obtained from these by time reversal.

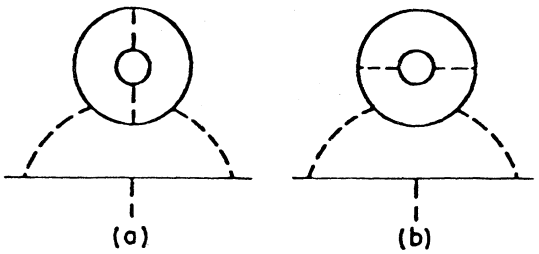

FIG. 3. Eighth-order vertices containing two closed electron loops, one within the other.

Subgroup I(c): diagrams containing two closed electron loops—one within the other. Three diagrams belong to this subgroup. Two are shown in Fig. 3. The third is obtained from Fig. 3(b) by charge conjugation.

Subgroup I(d): diagrams obtained by insertion of sixth-order (single electron loop) vacuum polarization subdiagrams in a second-order vertex. Fifteen diagrams belong to this subgroup. Eight are shown in Fig. 4. Each of A, C, D, E, and F and the time reversed diagram for E has a charged conjugated counterpart.

The contribution of subgroups I(a) and I(b) can be readily evaluated using the second- and fourth-order spectral functions for the photon propagator which are known analytically.[8,9] As the sixth-order photon spectral function is not known, the remaining 18 diagrams could not be evaluated similarly. Thus our first task was to construct an analogous sixth-order

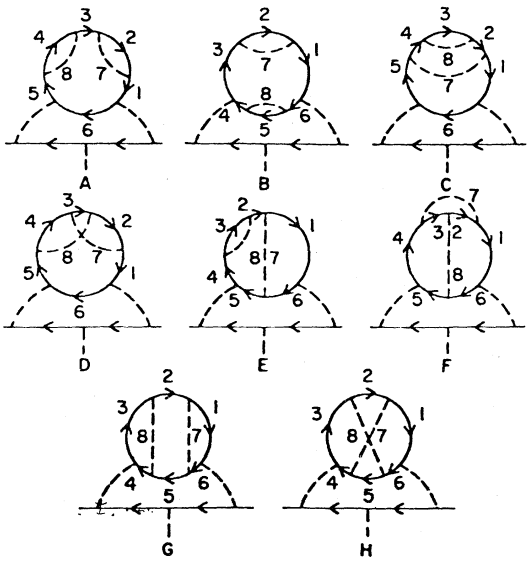

FIG. 4. Eighth-order vertices obtained by insertion of sixth-order (single electron loop) vacuum polarization subdiagrams in a second-order vertex.

TABLE I. Contributions of individual diagrams of Figs. 3 and 4 (factor η_i of 2 or 4 for asymmetric diagrams included).

Figure	$\eta_i \Delta M_i$	Residual renormalization terms
3(a)	0.011 40 (2)	$-2\Delta L_{2,P2} M_{2,P2}$
3(b)	0.001 72 (1)	$-2\Delta B_{2,P2} M_{2,P2}$
4A	0.044 56 (14)	$-4\Delta' B_2 M_{2,P4b} + 2(\Delta' B_2)^2 M_{2,P2}$
4B	0.028 39 (19)	$-2\Delta' B_2 M_{2,P4b} + (\Delta' B_2)^2 M_{2,P2}$
4C	−0.038 33 (5)	$-2\Delta' B_2 M_{2,P4b} + 2(\Delta' B_2)^2 M_{2,P2}$ $-2\Delta' B_{4b} M_{2,P2} - 2\Delta\delta m_{4b} M_{2,P2^*}$
4D	−0.027 40 (12)	$-4\Delta' L_2 \Delta M_{2,P4b} + 4\Delta' L_2 \Delta' B_2 M_{2,P2}$ $-2\Delta' B_{4a} M_{2,P2} - 2\Delta\delta m_{4a} M_{2,P2^*}$
4E	0.179 25 (43)	$-4\Delta' L_2 M_{2,P4b} + 8\Delta' L_2 \Delta' B_2 M_{2,P2}$ $-4\Delta' L_{4s} M_{2,P2} - 4\Delta' B_2 \Delta M_{2,P4a}$
4F	−0.061 93 (13)	$4(\Delta' L_2)^2 M_{2,P2} - 4\Delta' L_{4c} M_{2,P2}$ $-2\Delta' L_2 M_{2,P4a}$
4G	0.038 80 (14)	$3(\Delta' L_2)^2 M_{2,P2} - 2\Delta' L_{4l} M_{2,P2}$ $-2\Delta' L_2 \Delta M_{2,P4a}$
4H	0.023 52 (12)	$-2\Delta' L_{4x} M_{2,P2}$

function, which we achieved in a form convenient for numerical integration by making use of a parametric representation of Feynman amplitudes[10] and a specific method of renormalization[11] developed and applied successfully to the calculation of the sixth-order anomalous magnetic moment of the electron.[12] Details of this construction are described in a separate article.[13]

Our calculations are carried out in the Feynman gauge.

All numerical integrations were performed on the CDC 7600 at Brookhaven National Laboratory using the integration routine RIWIAD.[14] The results of numerical evaluation of individual integrals are summarized in Table I. Values of auxiliary integrals needed to obtain the contribution $a_I^{(8)}$ of group I diagrams to the electron anomaly are given in Table II. Combining these results we find

$$a_I^{(8)} = 0.0766(6)(\alpha/\pi)^4 . \tag{1.6}$$

This result was reported earlier in Ref. 15. The uncertainties in (1.6) and Tables I and II represent the 90% confidence limits estimated by the integration routine.

TABLE II. Auxiliary integrals—group I.

Term	Value	Defining equation
$M_{2,P2}$	0.015 687[a]	(3.6)
$M_{2,P2^*}$	−0.012 702[a]	(4.14)
ΔB_2	0.75	(4.15)
$\Delta M_{2,P4a}$	0.034 548 (12)	(3.18)
$2\Delta M_{2,P4b}$	0.041 864 (23)	(3.24)
$\Delta B_{4a} + 2\Delta L_{4c} + \Delta L_{4x}$	−0.513 8 (17)	(4.15)
$\Delta B_{4b} + 2\Delta L_{4s} + \Delta L_{4l}$	0.542 4 (6)	(4.15)
$\Delta\delta m_{4a}$	−0.301 5 (10)	(4.15)
$\Delta\delta m_{4b}$	2.208 1 (4)	(4.15)

[a]Exact values are $M_{2,P2} = \frac{119}{36} - \pi^2/3$ and $M_{2,P2^*} = \frac{16}{3} - 13\pi^2/24$.

In Sec. II we outline our calculation of the contributions from subgroups I(a) and I(b). In preparation for the discussion of subgroups I(c) and I(d), we present in Sec. III a very brief summary of the Feynman parametric-integral formulation of second- and fourth-order vacuum polarization loops given in Ref. 13 and of the integrals obtained when the loops are inserted in a vertex diagram. Based on Sec. III and the results for sixth-order vacuum polarization loops given in Ref. 13 we discuss the contributions of subgroups I(c) and I(d) in Sec. IV. Comments on the numerical integration are given in Sec. V.

II. CONTRIBUTION OF SECOND- AND FOURTH-ORDER VACUUM POLARIZATION LOOPS

For simplicity we shall omit the factor α/π and put the electron mass equal to unity throughout this article.

As is well known, the effect of a vacuum polarization loop insertion in a photon line is to give a (variable) mass to the photon propagator. To take advantage of this fact let us write the contribution to the second-order electron anomalous moment from the vertex diagram containing a virtual photon of

mass μ in the form

$$a^{(2)}(\mu)=\int_0^1 dy\frac{1-y}{W}\ , \tag{2.1}$$

where

$$W=1+\mu^2\frac{1-y}{y^2}\ . \tag{2.2}$$

If, in the photon line, we insert a gauge-invariant set of closed electron loops which is expressed by the renormalized vacuum polarization tensor

$$\Pi^{\mu\nu}(q)=(q^\mu q^\nu-g^{\mu\nu}q^2)\Pi(q^2)\ , \tag{2.3}$$

where

$$\Pi(q^2)=-q^2\int_0^1 dt\frac{\rho(t)}{q^2-4/(1-t^2)}\ ,\ \Pi(0)=0, \tag{2.4}$$

its contribution to the electron anomaly becomes

$$a=\int_0^1 dy(1-y)\int_0^1 dt\frac{\rho(t)}{W_t}\ , \tag{2.5}$$

where

$$W_t=1+\frac{4}{1-t^2}\frac{1-y}{y^2}\ , \tag{2.6}$$

$4/(1-t^2)$ being the mass of the virtual photon. If n such loops are inserted sequentially in the same photon line we obtain[16]

$$a=\int_0^1 dy(1-y)\left[\int_0^1 dt\frac{\rho(t)}{W_t}\right]^n\ , \tag{2.7}$$

which can be readily proved using the partial fraction decomposition

$$\frac{1}{x}\prod_{i=1}^n\frac{x}{x-a_i}=\sum_{k=1}^n\frac{1}{x-a_k}\prod_{i\neq k}\frac{a_k}{a_k-a_i}\ . \tag{2.8}$$

Formulas (2.5) and (2.7) enable us to calculate the contribution of vacuum polarization loops to the electron anomaly once the spectral function $\rho(t)$ is known. For the second and fourth orders, we have[8,9]

$$\rho_2(t)=\frac{t^2(1-t^2/3)}{1-t^2} \tag{2.9}$$

and

$$\begin{aligned}\rho_4(t)=\frac{2t}{3(1-t^2)}\Bigg[&\frac{(3-t^2)(1+t^2)}{2}\Bigg\{L(1)+\ln\left[\frac{1+t}{2}\right]\ln\left[\frac{1+t}{1-t}\right]\\&+2\left[L\left[\frac{1-t}{1+t}\right]+L\left[\frac{1+t}{2}\right]-L\left[\frac{1-t}{2}\right]\right]-4L(t)+L(t^2)\Bigg\}\\&+\left[\tfrac{11}{16}(3-t^2)(1+t^2)+\frac{t^4}{4}-\tfrac{3}{2}t(3-t^2)\right]\ln\left[\frac{1+t}{1-t}\right]\\&+t(3-t^2)\left[3\ln\left[\frac{1+t}{2}\right]-2\ln(t)\right]+\tfrac{3}{8}t(5-3t^2)\Bigg]\ ,\end{aligned} \tag{2.10}$$

with

$$L(t)=-\int_0^t\frac{dx}{x}\ln(1-x)\ . \tag{2.11}$$

The contributions of subgroups I(a) and I(b) are thus as follows.

Subgroup I(a). This is one of the few cases in the eighth order where the analytic result is known.[17] We repeat the calculation here as a check of our method. We start from

$$a^{(8)}_{\mathrm{I(a)}}=\int_0^1 dy(1-y)\left[\int_0^1 dt\frac{\rho_2(t)}{1+[4/(1-t^2)](1-y)/y^2}\right]^3\ , \tag{2.12}$$

where ρ_2 is given by (2.9). Carrying out the t integration we find

$$a^{(8)}_{\mathrm{I(a)}}=\int_0^1 dy(1-y)\left[-\frac{8}{9}+\frac{a^2}{3}+\left[\frac{a}{2}-\frac{a^3}{6}\right]\ln\left[\frac{a+1}{a-1}\right]\right]^3\ , \tag{2.13}$$

where

$$a=2/y-1\ . \tag{2.14}$$

By numerical integration we obtain

$$a^{(8)}_{\mathrm{I(a)}}=0.000\,876\,8(2)\,, \tag{2.15}$$

which is in excellent agreement with the analytic result[17]

$$a^{(8)}_{\mathrm{I(a)}}=151\,849/40\,824+\tfrac{32}{63}\zeta(3)-4\zeta(4)=0.000\,876\,865\cdots\,, \tag{2.16}$$

where ζ is the Riemann ζ function.

Subgroup I(b). The contribution of the six diagrams of this subgroup can be written as

$$a^{(8)}_{\mathrm{I(b)}}=2\int_0^1 dy(1-y)\int_0^1 ds\frac{\rho_2(s)}{1+[4/(1-s^2)](1-y)/y^2}\int_0^1 dt\frac{\rho_4(t)}{1+[4/(1-t^2)](1-y)/y^2}\,, \tag{2.17}$$

where ρ_2 and ρ_4 are given by (2.9) and (2.10). Numerical integration gives

$$a^{(8)}_{\mathrm{I(b)}}=0.015\,325(2)\,. \tag{2.18}$$

III. ANOMALOUS MOMENT CONTAINING PARAMETRIC FORMS OF VACUUM POLARIZATON LOOPS

In this section we summarize briefly the parametric forms of second- and fourth-order vacuum polarization loops and their contribution to the electron magnetic moment when inserted in a second-order vertex. Although analytic results are known in these cases, this is useful for illustrating our general procedure described in Sec. IV. Furthermore, these parametric formulas will be needed later in the renormalization of the integrals of subgroups I(c) and I(d).

For the second-order electron loops of Fig. 5(a) we can write the renormalized vacuum polarization tensor in the form

$$\Pi^{(2)}_{\mu\nu}(q)=(q_\mu q_\nu-g_{\mu\nu}q^2)\Pi^{(2)}(q^2)\,, \tag{3.1}$$

with[13]

$$\Pi^{(2)}(q^2)=\int(dz)\frac{D_0}{U^2}\ln\left[\frac{V_0}{V}\right], \tag{3.2}$$

where[18]

$$(dz)=dz_1dz_2\delta(1-z_{12})\,,$$
$$z_1\geq 0,\quad z_2\geq 0,\quad U=z_{12},\quad A_1=z_2/U,\quad V_0=z_{12}\,,$$
$$G=z_1A_1,\quad V=V_0-q^2G,\quad D_0=2A_1(1-A_1)\,. \tag{3.3}$$

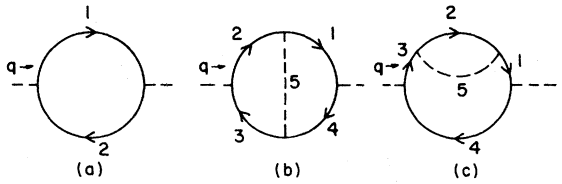

FIG. 5. Vacuum polarization diagrams of second and fourth orders.

Equation (3.2) can be rewritten in the form

$$\Pi^{(2)}(q^2)=q^2\int(dz)\int_0^1 dt\frac{D_0G}{U^2V_t}\,, \tag{3.4}$$

with

$$V_t=V_0-tq^2G\,. \tag{3.5}$$

If we note the similarity of (3.4) to the spectral representation (2.4), we can readily conclude that the contribution of (3.4) to the electron anomaly is[19]

$$a^{(4)}_{2,P2}=M_{2,P2}=\int_0^1 dy(1-y)\int(dz)\frac{D_0}{U^2}\ln\left[\frac{W}{W-1}\right], \tag{3.6}$$

where

$$W=1+\frac{V_0}{G}\frac{1-y}{y^2}\,. \tag{3.7}$$

In this form the relation between $M_{2,P2}$ and $\Pi^{(2)}$ of (3.2) is very transparent. This relation can be readily generalized to higher-order cases. With the variable change $z_1=(1+t)/2$ and integration by parts (3.6) can be rewritten as (2.5) (with $\rho\equiv\rho_2$).

The fourth-order vacuum polarization tensor has contributions from the diagram of Fig. 5(b) and from two diagrams of the form shown in Fig. 5(c). The former contribution, renormalized at $q=0$ but with subvertex divergences not yet explicitly removed, can be written as[13,20]

$$\Pi^{(4a)}(q^2)=\int(dz)\left[\frac{D_0}{U^2}\left[\frac{1}{V}-\frac{1}{V_0}\right]+\frac{D_1}{U^3}\ln\left[\frac{V_0}{V}\right]\right], \tag{3.8}$$

where[18]

$$
\begin{aligned}
&(dz)=dz_1dz_2dz_3dz_4dz_5\delta(1-z_{12345})\ ,\\
&U=z_5z_{1234}+z_{14}z_{23}\ ,\\
&B_{11}=z_{235},\ B_{12}=z_5,\ B_{22}=z_{145}\ ,\\
&A_1=(z_3B_{12}+z_4B_{11})/U,\ A_4=A_1-1\ ,\\
&A_2=(z_3B_{22}+z_4B_{12})/U,\ A_3=A_2-1\ ,\\
&V_0=z_{1234},\ G=z_1A_1+z_2A_2,\ V=V_0-q^2G\ ,\\
&D_0=(A_1+A_4)(A_2+A_3)-A_1A_4-A_2A_3\ ,\\
&D_1=(A_1A_2+A_3A_4)B_{12}-A_1A_4B_{22}-A_2A_3B_{11}\ .
\end{aligned}
\tag{3.9}
$$

This integral contains ultraviolet (UV) divergences arising from the subvertices $S'=\{2,3,5\}$ and $S''=\{1,4,5\}$. The divergent terms can be isolated by applying $K_{S'}$ and $K_{S''}$ operations[11,12] to the integrand of (3.8). For the $\{2,3,5\}$ vertex we find the divergence to be[13,21]

$$
K_{23}\Pi^{(4a)}=\int(dz)\frac{D_1'}{U'^3}\ln\frac{V_0'}{V'}\ ,
\tag{3.10}
$$

where

$$
\begin{aligned}
&U'=z_{14}z_{235},\ V_0'=z_{14}+z_{23}^2/z_{235}\ ,\\
&A_1'=z_4/z_{14},\ A_4'=A_1'-1,\ B_{22}'=z_{14}\ ,\\
&D_1'=-A_1'A_4'B_{22}',\ G'=z_1A_1'\ ,\\
&V'=V_0'-q^2G'\ .
\end{aligned}
\tag{3.11}
$$

A similar formula holds for $K_{14}\Pi^{(4a)}$. It is easily seen that (3.10) factorizes as

$$
K_{23}\Pi^{(4a)}=\hat{L}_2\Pi^{(2)}\ (\text{also } K_{14}\Pi^{(4a)}=\hat{L}_2\Pi^{(2)})\ ,
\tag{3.12}
$$

where $\hat{L}_2$ is the UV-divergent part of the vertex renormalization constant L_2,[22]

$$
\begin{aligned}
&L_2=\hat{L}_2+\Delta'L_2\ ,\\
&\hat{L}_2=\tfrac{1}{2}(\ln\Lambda-\tfrac{1}{4})\ ,\\
&\Delta'L_2=\ln\lambda+\tfrac{5}{4}\ ,
\end{aligned}
\tag{3.13}
$$

Λ and λ being the UV and infrared (IR) cutoffs, respectively.

Making use of (3.12) and (3.13), we can write the function

$$
\Pi_{\text{ren}}^{(4a)}=\Pi^{(4a)}-2L_2\Pi^{(2)}\ ,
\tag{3.14}
$$

which is obtained by a standard renormalization of the subvertices, as

$$
\Pi_{\text{ren}}^{(4a)}=\Delta\Pi^{(4a)}-2\Delta'L_2\Pi^{(2)}\ ,
\tag{3.15}
$$

where

$$
\Delta\Pi^{(4a)}=(1-K_{23}-K_{14})\Pi^{(4a)}
\tag{3.16}
$$

is free from UV divergences.

We are now ready to find the contribution of the sixth-order diagram of Fig. 6(a) to a_e. Going through steps analogous to (3.15) we find it to be[19]

$$
a_{2,P4a}^{(6)}=\Delta M_{2,P4a}-2\Delta'L_2M_{2,P2}\ ,
\tag{3.17}
$$

where

$$
\Delta M_{2,P4a}=\int_0^1dy(1-y)\int(dz)\left[\frac{D_0}{U^2V_0W}+\frac{D_1}{U^3}\ln\left[\frac{W}{W-1}\right]-\frac{D_1'}{U'^3}\ln\left[\frac{W'}{W'-1}\right]-\frac{D_1''}{U''^3}\ln\left[\frac{W''}{W''-1}\right]\right]\ ,
\tag{3.18}
$$

with

$$
W=1+\frac{V_0}{G}\frac{1-y}{y^2},\quad W'=1+\frac{V_0'}{G'}\frac{1-y}{y^2},\quad W''=1+\frac{V_0''}{G''}\frac{1-y}{y^2}\ .
\tag{3.19}
$$

The primed variables are given in (3.11) and the double-primed variables are analogously defined for the K_{14} UV subtraction.

The renormalized vacuum polarization term due to Fig. 5(c) can be written as

$$
\Pi_{\text{ren}}^{(4b)}(q^2)=\Delta\Pi^{(4b)}(q^2)-\Delta'B_2\Pi^{(2)}(q^2)\ ,
\tag{3.20}
$$

$$
\Delta\Pi^{(4b)}(q^2)=\int(dz)(1-K_S)\left[\frac{D_0}{U^2}\left[\frac{1}{V}-\frac{1}{V_0}\right]+\frac{q^2C_0}{U^2V}+\frac{D_1}{U^3}\ln\left[\frac{V_0}{V}\right]\right]\ ,
$$

where S is the self-energy subdiagram $\{2,5\}$ and

$$U=z_5z_{1234}+z_2z_{134},\quad V_0=z_{1234},\quad B_{11}=z_{25},\quad B_{12}=z_5,\quad B_{22}=z_{1345}\ ,$$
$$A_1=z_4B_{11}/U,\quad A_2=z_4B_{12}/U,\quad A_3=A_1,\quad A_4=A_1-1,\quad G=z_{13}A_1+z_2A_2,\quad V=V_0-q^2G\ , \tag{3.21}$$
$$D_0=(4A_1-A_2)A_4,\quad C_0=-A_1{}^2A_2A_4,\quad D_1=B_{12}A_1(A_1+3A_4)\ .$$

$\Delta' B_2$ is the UV-finite part of the wave-function renormalization constant B_2,[23]

$$B_2=\Delta' B_2+\hat{B}_2,\quad \hat{B}_2=-\tfrac{1}{2}(\ln\Lambda+\tfrac{5}{4}),\quad \Delta' B_2=\tfrac{3}{4}-\Delta' L_2\ . \tag{3.22}$$

V_0 and (dz) are the same as in (3.9).

The contribution of the diagram of Fig. 6(b) to the electron anomaly is then given by

$$a^{(6)}_{2,P4b}=\Delta M_{2,P4b}-\Delta' B_2 M_{2,P2}\ , \tag{3.23}$$

where

$$\Delta M_{2,P4b}=\int_0^1 dy(1-y)\int (dz)(1-K_2)\left[\frac{D_0}{U^2V_0W}+\frac{C_0}{U^2GW}+\frac{D_1}{U^3}\ln\left[\frac{W}{W-1}\right]\right]. \tag{3.24}$$

All quantities are defined in (3.21) except that W is given by (3.19) in terms of the appropriate V_0 and G.

The total contribution of the diagrams of Figs. 5(a) and 5(b) to the electron anomaly is thus

$$a^{(6)}_{2,P4}=a^{(6)}_{2,P4a}+2a^{(6)}_{2,P4b}=\Delta M_{2,P4a}+2\Delta M_{2,P4b}-\tfrac{3}{2}M_{2,P2}\ . \tag{3.25}$$

We have evaluated $\Delta M_{2,P4a}$ and $\Delta M_{2,P4b}$ numerically. The results are listed in Table II. The value of $a^{(6)}_{2,P4}$ calculated from (3.25) [0.052 88(3)] is in good agreement with the exact result 0.052 87. . . .[24]

IV. CONTRIBUTION OF SIXTH-ORDER VACUUM POLARIZATION LOOPS

Following the discussion of Sec. III, the contributions from the diagrams of subgroup I(c) (Fig. 3) can be readily calculated once the contributions from the sixth-order diagrams of Figs. 6(a) and 6(b) are known. Consulting the formulas (2.7) and (3.18) we find that the diagram of Fig. 3(a) gives

$$a^{(8)}_{2,P(4a,P2)}=\Delta M_{2,P(4a,P2)}+\text{ residual renormalization terms}\ , \tag{4.1}$$

with

$$\Delta M_{2,P(4a,P2)}=\int_0^1 dy(1-y)\int_0^1 dt\rho_2(t)\int (dz)(1-K_{S'}-K_{S''})\left[\frac{D_0}{U^2V_0W}+\frac{D_1}{U^3}\ln\left[\frac{W}{W-1}\right]\right], \tag{4.2}$$

where S' and S'' are the respective subvertices $\{2,3,5\}$ and $\{1,4,5\}$ in the diagram of Fig. 6(a). Also

$$W=1+\frac{V_0}{G}\frac{1-y}{y^2} \tag{4.3}$$

with

$$V_0=z_{1234}+\frac{4}{1-t^2}z_5\ , \tag{4.4}$$

where $4/(1-t^2)$ is the effective photon mass due to vacuum polarization and (dz), U, G, D_0, and D_1 are given by (3.9). Similarly the diagram of Fig. 3(b) contributes

$$a^{(8)}_{2,P(4b,P2)}=\Delta M_{2,P(4b,P2)}+\text{ residual renormalization terms}\ , \tag{4.5}$$

with

$$\Delta M_{2,P(4b,P2)}=\int_0^1 dy(1-y)\int_0^1 dt\rho_2(t)\int (dz)(1-K_s)\left[\frac{D_0}{U^2V_0W}+\frac{C_0}{U^2GW}+\frac{D_1}{U^3}\ln\left[\frac{W}{W-1}\right]\right], \tag{4.6}$$

where S is the subdiagram $\{2,5\}$ of Fig. 6(b), W is defined by (4.3) and (4.4) and U, G, D_0, C_0, and D_1 are given by (3.21). The results of numerical integration of (4.2) and (4.6) are listed in Table I.

The residual renormalization terms for these contributions, which express the difference between the stand-

ard and K_S renormalizations, can be written in terms of integrals corresponding to Feynman diagrams of lower orders. They are listed in the third column of Table I. In this column $\Delta L_{2,P2}$ and $\Delta B_{2,P2}$ are finite parts of the UV-divergent constants $L_{2,P2}$ and $B_{2,P2}$ corresponding to the vertex and self-energy diagrams of Fig. 7:

$$\begin{aligned}\Delta L_{2,P2}&=-469/216+2\pi^2/9=0.021\,949\cdots\ ,\\ \Delta B_{2,P2}&=419/108-7\pi^2/18=0.041\,450\cdots\ .\end{aligned}\tag{4.7}$$

From Table I and (4.7) we find that the contribution of the subgroup I(c) to the electron anomaly is

$$a^{(8)}_{\mathrm{I(c)}}=0.011\,13(2)\ .\tag{4.8}$$

Vacuum polarization terms arising from the loops in the diagrams of subgroup I(d) (Fig. 4) can all be written in the form[13,20]

$$\Pi^{(6)}_{\mathrm{ren}}(q^2)=\Delta\Pi^{(6)}(q^2)+\text{ residual renormalization terms }\ ,\tag{4.9}$$

where

$$\Delta\Pi^{(6)}(q^2)=\tfrac{1}{2}\int(dz)\prod_S(1-K_S)\left[\frac{D_0}{U^2}\left[\frac{1}{V^2}-\frac{1}{V_0{}^2}\right]+\frac{q^2}{U^2V^2}(B_0+q^2C_0)\right.$$

$$\left.+\frac{D_1}{U^3}\left[\frac{1}{V}-\frac{1}{V_0}\right]+\frac{q^2B_1}{U^3V}+\frac{D_2}{U^4}\ln\left[\frac{V_0}{V}\right]\right]\tag{4.10}$$

and

$$(dz)=\prod_{i=1}^{8}dz_i\,\delta\left[1-\sum_{i=1}^{8}z_i\right],\quad V_0=z_{123456},\quad V=V_0-q^2G\ .\tag{4.11}$$

G is determined by the individual diagram. The functions D_0, D_1, D_2, B_0, B_1, and C_0 were obtained using the algebraic computation program SCHOONSCHIP[25] and are listed in the Appendix of Ref. 13. The K_S operations for all UV-divergent subdiagrams S must be carried out in (4.10). The contributions to the electron anomaly due to the diagrams of Fig. 4 can then be written as

$$a^{(8)}_{2,P6i}=\Delta M_{2,P6i}+\text{ residual renormalization terms }\ ,\tag{4.12}$$

$$\Delta M_{2,P6i}=\tfrac{1}{2}\int_0^1dy(1-y)\int(dz)\prod_S(1-K_S)\left[\frac{-1}{U^2W^2}\left[\frac{D_0}{V_0{}^2}(1-2W)+\frac{B_0}{GV_0}(1-W)+\frac{C_0}{G^2}\right]\right.$$

$$\left.+\frac{1}{U^3W}\left[\frac{D_1}{V_0}+\frac{B_1}{G}\right]+\frac{D_2}{U^4}\ln\left[\frac{W}{W-1}\right]\right],\tag{4.13}$$

where W is given by (3.19) in terms of the appropriate V_0 and G.

The integrals $\Delta M_{2,P6i}$ are free from divergence and can be evaluated numerically. Their values (multiplied by the appropriate multiplicity factor η_i) are listed in the second column of Table I. The residual renormalization terms are listed in the third column of the same table. In this column $M_{2,P2^*}$ represents the magnetic-moment contribution of the counterterm diagram shown in Fig. 6(c).

Summing the contributions of diagrams A to H of Fig. 4 yields

$$a^{(8)}_{\mathrm{I(d)}}=\sum_{i=A}^{H}\eta_i\Delta M_{2,P6i}-4\Delta B_2\Delta M_{2,P4}+5(\Delta B_2)^2M_{2,P2}-2(\Delta L^{(4)}+\Delta B^{(4)})M_{2,P2}-2\Delta\delta m^{(4)}M_{2,P2^*}\ ,\tag{4.14}$$

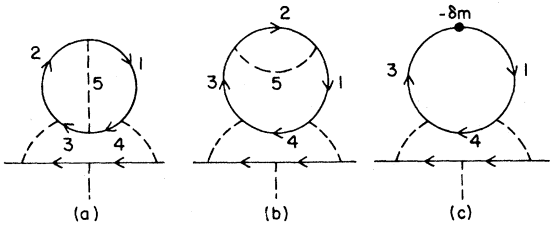

FIG. 6. (a) and (b) are sixth-order vertex diagrams containing fourth-order vacuum polarization loops. (c) is a diagram obtained by shrinking the electron self-energy subdiagram {2,5} of (b) to a point.

where

$$\eta_B=\eta_G=\eta_H=1\ ,$$
$$\eta_A=\eta_C=\eta_D=\eta_F=2\ ,\quad \eta_E=4\ ,$$
$$\Delta B_2=\Delta' B_2+\Delta' L_2=\tfrac{3}{4}\ ,$$
$$\Delta M_{2,P4}=\Delta M_{2,P4a}+2\Delta M_{2,P4b}\ , \tag{4.15}$$
$$\Delta L^{(4)}=\Delta L_{4x}+2\Delta L_{4c}+\Delta L_{4l}+2\Delta L_{4s}\ ,$$
$$\Delta B^{(4)}=\Delta B_{4a}+\Delta B_{4b}\ ,$$
$$\Delta\delta m^{(4)}=\Delta\delta m_{4a}+\Delta\delta m_{4b}\ .$$

The quantities in the last three lines of (4.15) are defined in Ref. 12. Their values are listed in Table II.

Using the numerical values listed in Tables I and II we obtain

$$a^{(8)}_{\mathrm{I(d)}}=0.049\,28(57)\ . \tag{4.16}$$

Finally, collecting the results (2.15), (2.18), (4.8), and (4.16) we obtain the contribution of 25 Feynman diagrams of group I to the electron anomaly a_e given in (1.6).

V. COMMENTS ON THE NUMERICAL INTEGRATION

One of the problems associated with Monte Carlo numerical integration of integrands involving point-by-point cancellation of divergent pieces is a hardware-dependent feature—the limits on the size of a number the computer can handle in any operation. A run may terminate with a register overflow if the integration routine samples in a divergent region and attempts to evaluate a divergent term before it has a chance to compute the corresponding subtraction term appearing later in the integrand. In our formulation, divergences (both UV and IR) are associated with regions where some Feynman parameters $z_i\to 0$. Hence, for certain z_i (or sums of z_i) the integration routine was prevented from sampling in a region $0\le z_i\le 10^{-12}$. The value of 10^{-12} was chosen empirically.

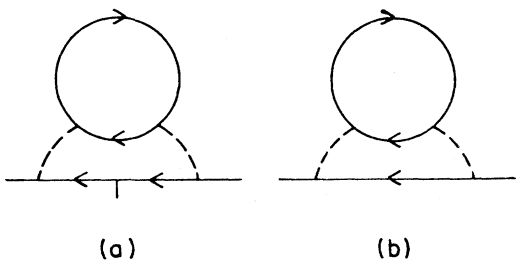

FIG. 7. Fourth-order vertex and electron self-energy diagrams containing a second-order vacuum polarization loop.

In addition, inspection of (4.2)–(4.4) reveals that $t\simeq 1$ and $y\simeq 1$ (perhaps in combination with certain Feynman parameters $z_i\to 0$) are regions that could potentially lead to a computer register overflow. This was found to be the case for the integrals of the diagrams of Figs. 2(a) and 2(b). Both were run with the regions $1-t<10^{-12}$ and $1-y<10^{-12}$ excluded.

Errors caused by such omissions of the integration domain are of order 10^{-12} and hence completely negligible. To see this let M be the unrenormalized integral corresponding to a Feynman diagram G with divergent subdiagrams $S,S',S'',\ldots$. Then the integral

$$(1-K_{S'})(1-K_{S''})\cdots M \tag{5.1}$$

is free from all divergences except a logarithmic one associated with the subdiagram S. Suppose S consists of the lines $1,2,\ldots,m$, and $z_1,z_2,..,z_m$ are the corresponding Feynman parameters. The divergence of (5.1) arises from the subdomain of integration

$$0\le z_1+z_2+\cdots+z_m\le z_S\ , \tag{5.2}$$

where z_S can be chosen as small as one wishes. In this domain the "phase space" is of order z_S^m and the integrand of (5.1) must behave as z_S^{-m} in order to generate a logarithmic divergence. If we now apply $1-K_S$ to (5.1) the integrand of the convergent integral

$$(1-K_S)(1-K_{S'})\cdots M \tag{5.3}$$

behaves as z_S^{-m+1} in the domain (5.2). This means that the contribution to the integral (5.3) from the domain defined by (5.2) is of order z_S, provided that the roundoff errors are under control.

Except for the integrands for Figs. 2(a) and 2(b), the final run for all diagrams consisted of a maximum of 2×10^5 subcubes (each subcube containing two sampling points) in the hypervolume defined by the range of integration (minus the excluded regions) for each iteration of the integral, with numbers of

iterations ranging from 5 to 10 depending on convergence rate and a time limit cutoff. The integrals for Figs. 3(a) and 3(b) were run with a maximum of 5×10^4 subcubes for each of 10 iterations. For the longer integration runs, computing times ranged from 5 to 10 minutes on the CDC 7600.

ACKNOWLEDGMENTS

We wish to thank Dr. R. F. Peierls and Brookhaven National Laboratory for generous support of our work. This work was supported in part by the National Science Foundation.

---

*Present address: Courant Institute of Mathematical Sciences, New York University, New York, NY 10012.

[1]P. B. Schwinberg, R. S. Van Dyck, Jr., and H. G. Dehmelt, Phys. Rev. Lett. 47, 1679 (1981).

[2]The quantity enclosed in parentheses represents the uncertainty in the final digits of a numerical value.

[3]The coefficient C_2 includes the contribution of the muon vacuum polarization loop

$$a_e(\text{muon})=2.8\times10^{-12}\ ,$$

but not the hadronic contribution [$\sim1.6(2)\times10^{-12}$], or weak-interaction effect (0.05×10^{-12}, according to the standard Weinberg-Salam model). The τ vacuum polarization loop contribution (0.01×10^{-12}) is negligible compared to these. See T. Kinoshita, in *New Frontiers in High Energy Physics,* edited by B. Kursunoglu, A. Perlmutter, and L. F. Scott (Plenum, New York, 1978), p. 127.

[4]M. J. Levine, H. Y. Park, and R. Z. Roskies, Phys. Rev. D 25, 2205 (1982).

[5]E. R. Williams and P. T. Olsen, Phys. Rev. Lett. 42, 1575 (1979).

[6]M. J. Levine, R. Roskies, and E. Remiddi, private communications.

[7]T. Kinoshita and W. B. Lindquist, Cornell Report No. CLNS-374, 1977 (unpublished).

[8]G. Källén and A. Sabry, K. Dan. Vidensk. Selsk. Mat.-Fys. Medd. 29, No. 17 (1955).

[9]J. Schwinger, *Particles, Sources and Fields* (Addison-Wesley, Reading, Mass., 1973), Vol. 2, p. 407.

[10]P. Cvitanović and T. Kinoshita, Phys. Rev. D 10, 3978 (1974).

[11]P. Cvitanović and T. Kinoshita, Phys. Rev. D 10, 3991 (1974).

[12]P. Cvitanović and T. Kinoshita, Phys. Rev. D 10, 4007 (1974).

[13]T. Kinoshita and W. B. Lindquist, preceding paper, Phys. Rev. D 27, 853 (1983).

[14]For a description of RIWIAD see, for instance, B. E. Lautrup, in *Proceedings of the Second Colloquium on Advanced Computer Methods in Theoretical Physics, Marseille, 1971,* edited by A. Visconti (University of Marseille, Marseille, 1971).

[15]T. Kinoshita and W. B. Lindquist, Phys. Rev. Lett. 47, 1573 (1981).

[16]T. Kinoshita, Nuovo Cimento 51B, 140 (1967).

[17]J. A. Mignaco and E. Remiddi (unpublished); M. A. Samuel, Report No. NBI-HE-77-31, 1977 (unpublished).

[18]For brevity we use the notation $z_{12\cdots n}=z_1+z_2+\cdots+z_n$.

[19]See T. Kinoshita and W. B. Lindquist, following paper, Phys. Rev. D 27, 877 (1983) (Appendix) for a discussion of the notation employed for diagrams and amplitudes. The sixth-order polarization loops used for labeling diagrams are illustrated in Figs. 3 and 4. The loops in 3(a) and 3(b) are labeled $\Pi^{(4a,P2)}$ and $\Pi^{(4b,P2)}$, respectively. Those in 4(*A*) to 4(*H*) are labeled $\Pi^{(6A)}$ through $\Pi^{(6H)}$.

[20]The diagram of Fig. 5(b) is not gauge invariant by itself and hence the corresponding amplitude cannot be written in the form (2.3). However, since gauge-dependent terms cancel when the contributions of Figs. 5(b) and 5(c) are summed, we can treat individual amplitudes such as $\Pi^{(4a)}$ as if they are gauge invariant. This comment applies to all gauge-invariant sets of diagrams.

[21]In discussing a particular subdiagram S of a diagram, we prefer to label the K_S operation that isolates the UV singularity due to S by the electron lines running through S. Thus for the $S'=\{2,3,5\}$ subvertex of Fig. 5(b) the associated $K_{S'}$ operation is labeled K_{23}.

[22]See formulas (3.13) and (3.14) of Ref. 12.

[23]See formulas (3.22) and (3.23) of Ref. 12.

[24]J. A. Mignaco and E. Remiddi, Nuovo Cimento 60A, 519 (1969).

[25]H. Strubbe, Comput. Phys. Commun. 8, 1 (1974); 18, 1 (1979).